Analyst

Microfluidic Approach for the Detection of Uric Acid through the Electrical Measurement of Atomically Thin MoS_2 Field-Effect Transistor

Journal:	*Analyst*
Manuscript ID	AN-ART-05-2023-000772.R1
Article Type:	Paper
Date Submitted by the Author:	27-Jun-2023
Complete List of Authors:	Nasiruddin, Md; Tohoku University, Chemistry Waizumi, Hiroki; Tohoku University, Dept. of Chemistry Takaoka, Tsuyoshi; Tohoku Daigaku, Institute of Multidisciplinary Research for Advanced Materials Wang, Zhipeng ; Tohoku University, Chemistry Sainoo, Yasuyuki; Tohoku University - Katahira Campus, Institute of Multidisciplinary Research for Advanced Materials Mamun, Muhammad Shamim Al; Khulna University, Chemistry Ando, Atsushi; National Institute of Advanced Industrial Science and Technology, Nanoelectronics Research Institute FUKUYAMA, MAO; Tohoku University, Institute of Multidisciplinary Research for Advanced Materials; Hibara, Akihide; Tohoku University, Institute of Multidisciplinary Research for Advanced Materials Komeda, Tadahiro; Tohoku University, Institute of Multidisciplinary Research for Advanced Materials

Microfluidic Approach for the Detection of Uric Acid through the Electrical Measurement of Atomically Thin MoS_2 Field-Effect Transistor

Md Nasiruddin,[1] Hiroki Waizumi,[1] Tsuyoshi Takaoka,[2] Zhipeng Wang,[1] Yasuyuki Sainoo,[2] Muhammad Shamim Al Mamun,[3] Atsushi Ando,[4] Mao Fukuyama,[2] Akihide Hibara,[2] and Tadahiro Komeda[2,5]*

[1] Department of Chemistry, Graduate School of Science, Tohoku University, Aramaki-Aza-Aoba, Aoba-Ku, Sendai 9808578, Japan

[2] Institute of Multidisciplinary Research for Advanced Materials (IMRAM, Tagen), Tohoku University, 2-1-1, Katahira, Aoba-Ku, Sendai 9800877, Japan

[3]Chemistry Discipline, Khulna university, Khulna-9208, Bangladesh

[4] National Institute of Advanced Industrial Science and Technology, 1-1-1 Umezono, Tsukuba, Ibaraki 305-8568, Japan

[5]Center for Spintronics Research Network, Tohoku University, 2-1-1 Katahira, Aoba-ku, Sendai 980-8577, Japan

Email: tadahiro.komeda.a1@tohoku.ac.jp

Abstract

There is a demand for biosensors working in vivo conditions, which requires significant device size and endurance miniaturization in solution environments. We demonstrated the detection of the uric acid (UA) molecule, a marker of diseases like gout, whose continuous monitoring is demanded in a medical diagnosis. We used the field effect transistor (FET) composed of an atomically thin transition metal dichalcogenides (TMDs) channel. The sensor detection was carried out in the solution environment, for which we protected the electrodes of the source and drain from the solution. A microfluidic channel controls the solution flow that can realize evaporation-free conditions and provide an accurate concentration and precise measurement. We detected a systematic change of the drain current with the concentration of the UA in isopropyl alcohol (IPA) solvent with a detection limit of 60 nM. The sensor behavior is reversible, and the drain current returns to its original value when the channel is washed with pure solvent. The results demonstrate the feasibility of applying the MoS_2-FET device to the UA detection in solution, suggesting the possible use in the solution environment.

Introduction

The lab-on-a-chip (LOC) technology attracts attention, including sensor integration and operation under *in-vivo* circumstances.[1,2] Transition metal dichalcogenides (TMD) is an ideal channel material for such applications due to their excellent properties as thin channel material,[3-8] such as high carrier mobility, a small number of dangling bonds, high surface-to-volume ratio, high stability, high on/off current ratio, and biocompatibility. Significantly, due to the high surface-to-volume ratio, the adsorption of foreign atoms or molecules modulates the FET's electronic property,[9] and can be good sensors of bio and environmental materials.[10,11] In addition, MoS_2 changes the band structure from the indirect band gap in the bulk state to the direct one in the thin layer.[12] This should contribute to the broader application domain compared to zero bandgap graphene and other traditional MOSFET cases.[13]

As a target biomolecule for biosensing, we consider uric acid (2,4,6-trihydroxypurine, UA), the final product of purine nucleotides in human sputum metabolism and exists in urine or serum released by the kidney and digestive system. The production and release of UA must maintain an equilibrium concentration (120-480 μM) in the serum.[14,15] Elevated levels of UA may cause several diseases, including gout,[16] cardiovascular problems,[17] hyperuricemia, renal disease, and Lesch-Nyhan syndrome.[18] Thus, monitoring the concentration of UA in the biological system is mandatory for the diagnosis. A simple, selective, and sensitive UA detection system is demanded for medical and diagnostic purposes.

Since the pioneering work by Offer in the 19th century, clinical analysis methods have been developed for the detection of the UA molecule, such as chemiluminescence,[19,20] spectrophotometry,[21] high-performance liquid chromatography (HPLC),[22] fluorometry,[23] electrochemical methods,[24,25] and capillary electrophoresis.[26] Nevertheless, these processes have several drawbacks, such as complex sample preparation, bulky instruments, and lengthy measurement time; further development of analysis techniques is required.

The TMD-FET-based sensor has the advantage of miniaturization, whose device size can be μm and can be operated in the body condition. In addition, we should stress that MoS_2 FET has a much lower limit of molecule detection than conventional sensors.[27] For the UA

detection limit, Wu and coworkers utilized a silver nanoprism which has a linear response between 1 μM to 40 μM with a limit of detection of 0.7 μM.[28] A MoS_2-based electrochemical sensor is claimed to have a linear response starting from 5 μM.[29] However, UA of a minor concentration in the nM range affects the emotional response to stress in mental health.[30] The high sensitivity can be realized especially for the structure where the bare channel is exposed to molecules compared with the channel covered with a protective layer.

At the same time, there are several concerns about the disadvantages of the TMD-FET device for biosensors, including the detection specificity and stability. For the former, the material selection of the EC probe has been discussed for many years. The use of a similar technique is more complex in the TMD-FET. Nevertheless, there is rapid progress in the functionalization of the channel utilizing the host-guest reaction for the atomic scale channel FET devices, which contributes to specifying the target molecule. Also, the formation of the protective layer on the channel prevents direct interaction with the thin channel, which will contribute to the stability of the FET. The formation of the protection layer has to compromise with the high sensitivity of the bare channel sensor.

Although the sensor behavior of TMD-FET is studied for a wide variety of molecules, the studies are executed mainly in vacuum and gas environments. A limited number of studies conducted in a solution environment primarily utilize a small volume of a droplet placed on the surface of the channel, which is open to the atmosphere, making less precise results from the solvent's evaporation. Microfluid platform controls solution flow in the sub-mm dimension and provides various advantages for biomaterial sensing.[31-33]A microfluidic sensing platform has several potential advantages, such as a small amount of analyte and high throughput detection. Moreover, the evaporation of the solution is almost negligible as the solution passes under the microchannel. In case the solution is changed, it can realize a quick switch. It can provide high accuracy, reproducibility, and achieved repeatability.[32,34,35]

In this report, we fabricated MoS_2-FET equipped with a microfluid channel to control the solution that flows on the bare channel layer of MoS_2. The drain and source electrodes are protected from contact with the solution. A microfluidic channel controls the solution flow that can realize evaporation-free conditions and provide an accurate concentration and

precise measurement. Our device especially combines the microfluidic and non-protected channels to realize a lower detection limit. We detected a systematic change of the drain current with the concentration of the UA in isopropyl alcohol (IPA) solvent with a detection limit of 60 nM, which is low enough for the diagnosis purpose. The sensor behavior is reversible, and the drain current returns to its original value when the channel is washed with pure solvent. The results demonstrate the feasibility of applying the MoS_2-FET device to UA detection, suggesting the possible use in the solution environment.

Experimental Section

Device fabrication

We fabricated MoS_2-FET, using MoS_2 flakes of four monolayer thicknesses as the channel of the FET. The flakes were transferred on the SiO_2 (285 nm)/pp++ Si(001) substrate by the Scotch® tape method, with the technique we described in our previous reports.[36] The electrodes for the source and drain are made of Au, which has a good electrical conductivity. However, the adhesiveness to the SiO_2 substrate and the Ohmic contact with the MoS_2 flake are the issues to be solved. Das and coworkers reported that Ti and Sc are suitable metals as interface materials from these viewpoints.[37] We use Ni in the interface layer, which has adhesiveness to the SiO_2 surface and good Ohmic contact with the MoS_2 surface.

We modified the device so that the solution contacts only the channel in a controlled manner. First, we coated the device with a poly(methyl methacrylate) (PMMA) A6 (Kayaku Advanced Materials, JAPAN) layer of 550 nm thickness, which is usually used for electron resist. To prevent the solution's contact with electrodes, we made a vertical hole (diameter of 1 μm) through the PMMA in the middle of the channel using electron lithography. We also removed PMMA from a part of the electrode pads for the source and drain to provide suitable contact for the electric measurement.

A microfluidic tank was constructed with PDMS, which has a length of 3180 μm and a height of 1100 μm, and a flow area of 50 μm (width) × 40 μm (height). The solution is introduced from a capillary, and a syringe pump controls the velocity of the solution flow. In this experiment, we use the flow rate of 100 μl/hour (flow speed of 14 mm/s). An optical

microscope of the microfluidic channel with the source and drain electrodes is shown in Fig. 1(a). The schematic drawing of the cross-section is shown in Fig. 1 (b).

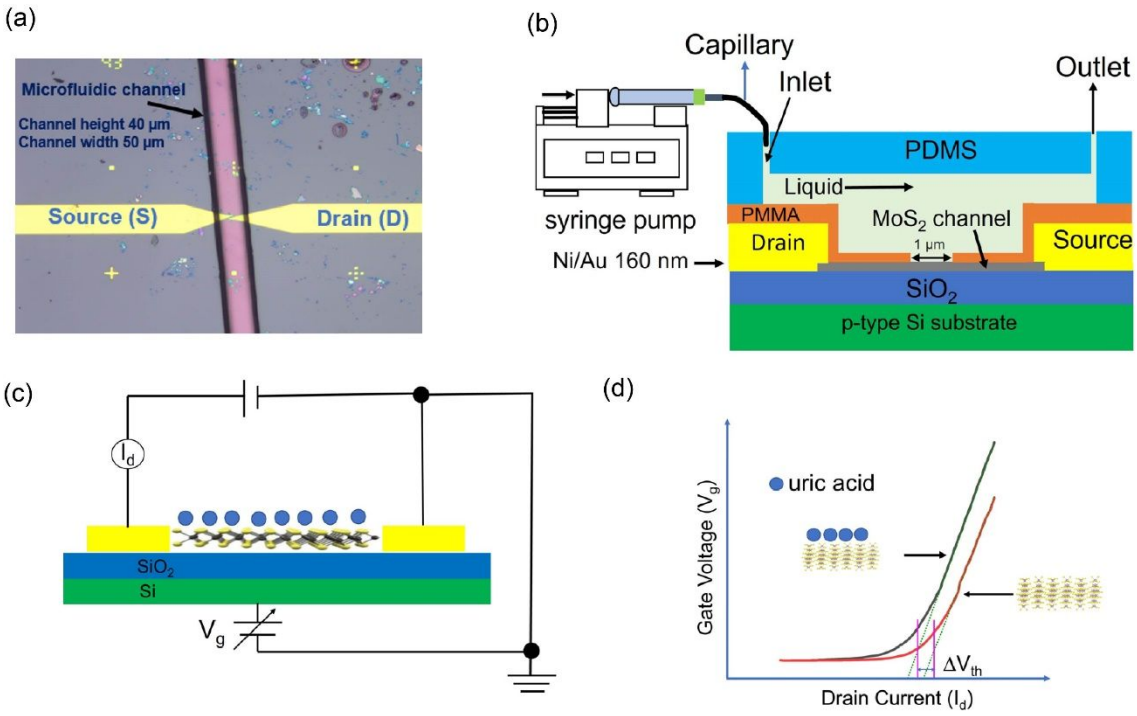

Fig. 1 (a) Optical picture showing the PDMS channel. (b) Schematics of the MoS_2-FET device with PMMA via hole and PDMS microfluidic platform. (c) Illustration of the FET property measurement of the drain current (I_d) and gate voltage (V_g). (d) Threshold voltage determination from the I_d-V_g curve and its shift ΔV_{th} with molecule adsorption.

Solution preparation and surface functionalization

UA (Sigma-Aldrich) solvent is formed using IPA. We carried out a long sonication process to make a homogeneous solution using an ultrasonic liquid processor (Qsonica, USA). The solution was pushed by a motorized syringe pump, which flowed through a capillary tube. Throughout this experiment, the flow rate of the solution was maintained at 100 μL/hour.

The operation principle of the MoS_2-FET biosensor

We illustrate the measurement system of the electric property of the MoS_2-FET in Fig. 1 (c), in which the gate voltage is applied from the substrate of highly doped Si. The change of the FET property by the molecule adsorption is estimated by observing the source−drain current (I_d) vs. gate voltage (V_g), which we call I_d-V_g curve [Fig. 1 (d)]. The I_d-V_g curve of a standard FET shows a linear and rapid increase at the threshold voltage (V_{th}). We estimated the voltage by fitting the linear increase part by a line and the interception voltage for I_d=0. ΔV_{th} corresponds to the change of the threshold voltage.

VASP calculation

The first-principle calculations were performed using the Vienna Ab initio Simulation Package (VASP) code, employing a plane wave basis set and projector augmented-wave (PAW) potentials to describe the valence electron behavior.[38,39] A generalized gradient approximation (GGA) using the Perdew-Burke-Ernzerhof (PBE) exchange-correlation potential was used.[40] The kinetic energy cutoff for the plane wave basis was set at 400 eV. The positions of the atoms in the UA and the MoS_2 slab were optimized without any constraint until the force on individual atoms and energy difference between iterations became smaller than 0.02 eV/Å and 10^{-5} eV, correspondingly. The structures and charge distributions were visualized by using the VESTA application.[41]

Results and discussion

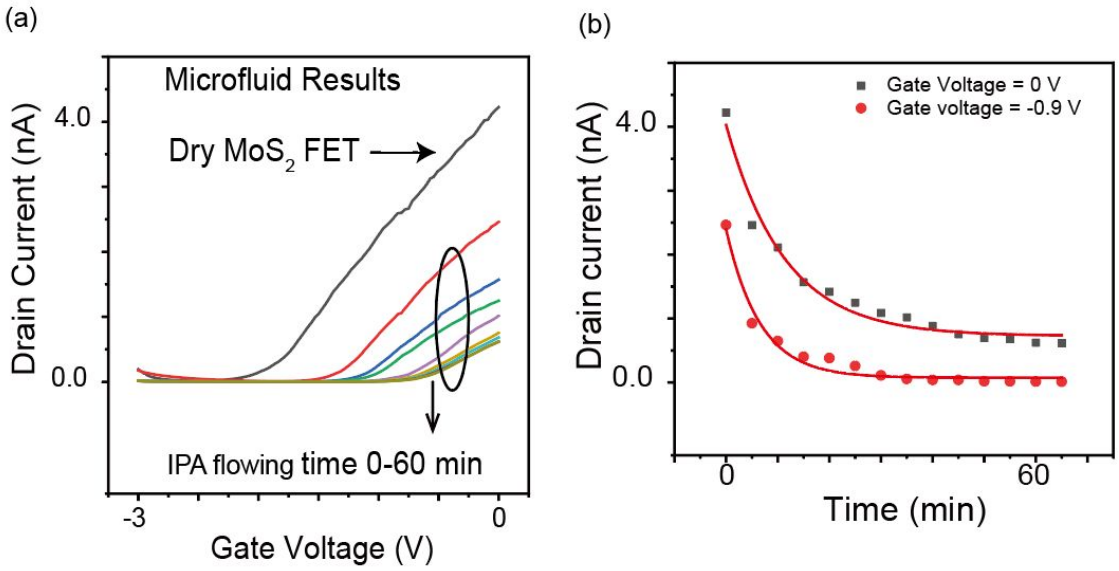

Fig. 2 Microfluidic results of the MoS_2-FET. (a) I_d-V_g data for the dry MoS_2 pristine and at IPA flow conditions onto the MoS_2 at 5 minutes intervals. The device stabilization process was depicted. (b) I_d vs. immersion time in IPA flow at two gate voltages (0 V and -0.9 V). A solid red curve indicates the fitting result (see main text).

In Fig. 2 (a), we show the change of the I_d-V_g curve when the MoS_2 channel contacts with the IPA. The solution flows in the microfluidic channel at 100 μL/hour. We used a moderate range of -3 to 0 V gate voltage to prevent damaging the channel with the high gate voltage. The curves are obtained every five minutes, and we see the gradual change of I_d-V_g plots until it saturates after 50 min. The curves shift to the positive voltage direction, suggesting the electron acceptor-like behavior of the IPA solution. The time required to reach the saturation value (50 min) is long, and the mechanism is not precise. The last curve represents the stabilized plot.

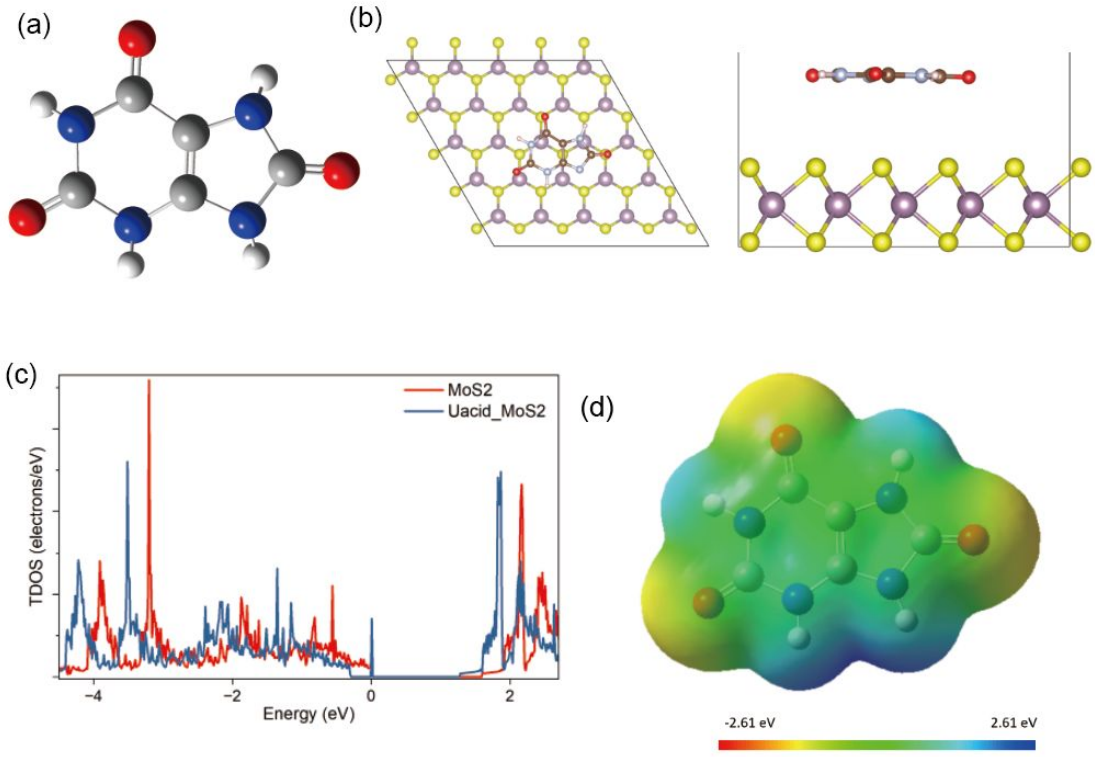

Fig. 3 (a) Molecule model of UA Atoms are represented as spheres with color coding: oxygen (red), hydrogen (white), carbon (grey), and nitrogen (blue). (b) Optimized adsorption configuration of UA on MoS_2 surface terminated by S layer. (c) The density of states before (red line) and after (blue) the adsorption of UA molecule. (d) Color mapping of the electrostatic potential mapping of an isolated UA molecule.

After stabilizing the FET property with the IPA flow in the microfluid channel, we switch the solution from pure IPA to UA solution by changing the syringe. The molecular model of UA is shown in Fig. 3 (a). The molecule consists of three oxygen atoms and four N atoms. Pullman and coworkers reported that the UA could be a suitable electron donor where the HOMO level is at a higher energy level.[42] We calculated UA's electronic structure after adsorbing on the MoS_2 surface by VASP, in which no IPA environment was considered. The optimized structure is shown in Fig. 3 (b), and we found that a flat-lying UA configuration is energetically stable. The total density of state (TDOS) is plotted before and after the adsorption of the UA molecule. All features of density-of-states of the MoS_2 substrate, shown by the red curve, shift to the higher binding energy (left-hand side). The electron donation

from the molecule to the MoS_2 can explain the shift. By this electron transfer, more electrons must be contained in the MoS_2 electronic states, pushing the states to the higher binding energy sides. This calculation supports the previous report by Pullman et al.[42] The electrostatic potential mapping is shown in Fig. 3 (d), and the electron accumulation can be observed at the oxygen atom positions.

The I_d-V_g curve monitors the change of the FET property by the existence of the UA solution at the channel surface. In Fig. 4 (a), we illustrate the evolution of the curves when UA solution with different concentrations flows in the microfluid channel. The bottom curve is obtained after the I_d-V_g curve is stabilized in pure IPA flow, as demonstrated in Fig. 2 (a). We exchanged the syringe, and the concentration of the UA solution was sequentially elevated.

We see an increase of I_d at each gate voltage with the concentration of the UA solution, where the shift can be identified with a concentration as low as 60 nM. The change indicates that the UA molecules work as electron donors to the MoS_2 FET. We numerically estimate the shift of the curves by calculating the threshold voltage of the I_d-V_g curve. For example, the threshold voltage changes to -0.843 V when the concentration of 60 nM is used from -0.658 V for the pure IPA case. As uric acid concentration increases to 300 nM and 1 μM, V_{th} moves to the left-hand side.

The V_{th} shift, estimated with a method shown in Fig. 1 (d) as a function of the UA concentration, is summarized in Fig. 4 (b). The V_{th} change can be fitted by a linear function with concentration. The solid red line in the figure shows the fitting result, which has a slope of 1.22 V per 1 μM where R-square [the coefficient of determination (COD)] is estimated as 98 %.

The behavior can be explained by the electron-donor character of the UA molecule, which works as the *n*-type dopant. The V_{th} shift is proportional to the amount of the transferred charge. A simple Langmuir model of the adsorption of the UA molecule on the MoS_2 surface can account for the linear dependence of the V_{th} shift on the concentration.[43,44] The coverage is less than a monolayer in the model. The number of adsorption sites is assumed to be either occupied by a UA molecule or empty. In an equilibrium condition, the

number of molecules that adsorb on and desorb from the surface should be equal. The coverage can be expressed as

$\theta=\eta/(1+\eta)$ ----(1)

where $\eta= p_a f_0 / n$ with f_0 as the number of molecules that hit the adsorption site per second, p_a as the sticking coefficient, and n as the desorption probability of a single adsorbate per second. The parameter f_0 is proportional to the UA concentration. With a small η, the UA coverage, θ deduced above, shows a small value and can be approximated as a linear increase with the concentration. Thus, the Langmuir model can account for the linear V_{th} behavior by assuming that the V_{th} shifts linearly with the UA coverage by a uniform charge transfer from each adsorbate.

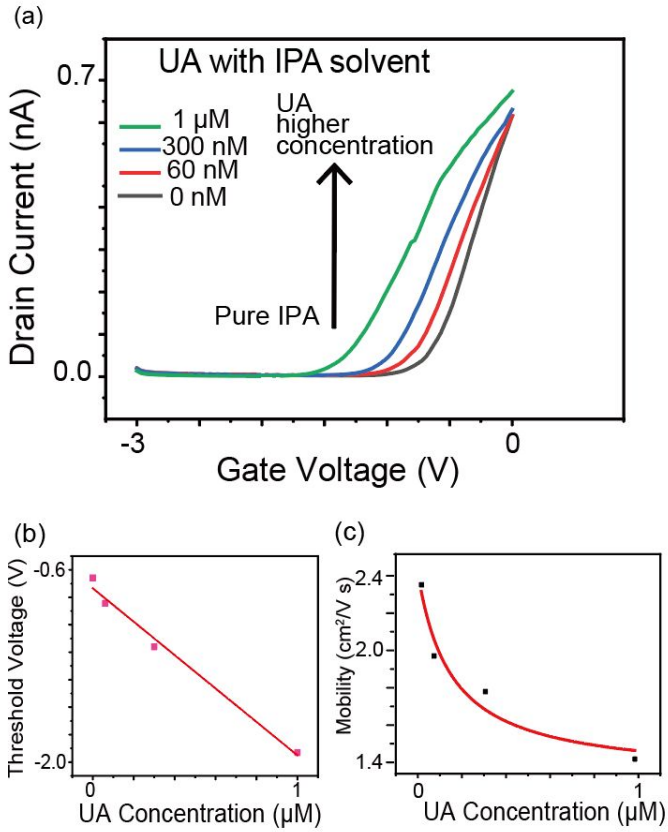

Fig. 4 (a) I_d-V_g changes with the UA concentration in IPA solvent. The bottom curve corresponds to the one after stabilization in IPA in Fig. 2 (a). (b) The shift of V_{th} as a function of the UA concentration. The experimental data are solid dots; the line shows the linear fitting result. (c) Calculated mobility vs. UA concentration; solid squares for the data, and the solid line is the fitting result.

The field effect mobility is one of the critical parameters for the characterization of two-dimensional semiconductor materials. The mobility can be estimated using the following equation,

$$\mu_{EF} = g_m \frac{L_{ch}}{W_{ch} C_{ox}} \frac{1}{V_d}$$

where $g_m = \frac{dI_d}{dV_g}$ is the transconductance, C_{ox} is the gate capacitance (1.12×10^{-8} F cm^{-2} for 285 nm SiO_2),[45] L_{ch} and W_{ch} are the MoS_2 channel length and width, respectively, and V_d is the drain voltage. In this experiment, L_{ch} of 7.8 μm, W_{ch} of 5.9 μm, and V_d of 50 mV are measured.

The calculated μ_{EF} is plotted as a function of the UA concentration in Fig. 4 (c). The mobility decreases with the UA concentration, but the plot is not linear as seen for the ΔV_{th}. The decrease in mobility can be accounted for by the non-periodic potential formed by the uric acid molecules adsorbed on the surface, which scatter the drain current. The curve can be fitted with equation (1) as indicated by the solid red line in Fig. 4 (c). The discrepancy in the appearance of the threshold voltage change in Fig. 4 (b) can be explained by a model in which the effect of a single adsorbed molecule for mobility is more significant compared to the threshold voltage due to the long-range nature of the scattering potential.

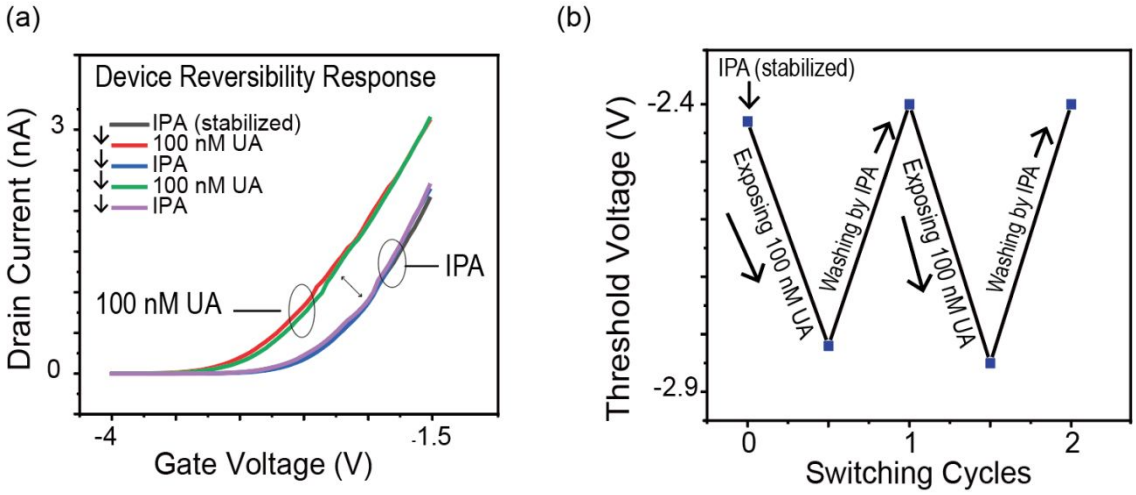

Fig. 5 (a) I_d-V_g variation when the solution switches between the pure IPA and the UA solution of 100 nM. (b) ΔV_{th} plot when the syringe solution cycled between 100 nM UA and washing IPA.

For applying the device to the sensor, the reproducibility of the electric change is critical. To show the reproducibility, we executed cycles of switching the syringe solution between 100 nM UA solution and the washing IPA. The results are shown in Fig. 5 (a) as the I_d-V_g changes and as the ΔV_{th} plot in Fig. 5 (b). In the washing process, we kept the flow of pure IPA at 100 μL/hour flow rate for 30 min. The I_d-V_g curve shape and the ΔV_{th} value return to the initial ones, indicating a robust cycle property. We confirmed that the devices' survival time is more than days when an adequate flow velocity is selected (100 μL/hour) is used in our microfluidic experiment. Some research studies claimed that exposure to organic solvents may swell PDMS.[46] Nevertheless, PDMS swelling has not occurred in our study. We provide an additional chemical analysis of the UA molecules transferred onto the MoS_2 surface in Supplemental Information.

So far, we show the results obtained using the IPA as a solvent while the actual working environment is in water. This is due to the problems when the device is combined with the water. Similar issues have been discussed previously.[47] It is pointed out that the electrical measurement in a liquid environment frequently results in partially destroying the channel material. Also, high drain voltage and high gate voltage ramps often cause device instability. In addition, prolonged contact with the solution can impose voltage stress, which in turn causes electrochemical corrosion inside the channel layers. Meanwhile, the solution flow can cause damage to the device. Inhomogeneous or turbulent flow should form large bubbles striking the MoS_2 flake. In addition, the interpenetration of solution into the interface between MoS_2 and the Si/SiO_2 substrate might damage the channel.

We made additional designs in our device to solve these issues. One is a PMMA coating on the metal electrode portions to prevent Ni/Au electrodes from directly contacting molecular solutions. This coating is expected to lower the leakage current and dielectric constant and enhance the device's dielectric strength and stability.[48] Si/SiO_2 substrate was also rendered flat by the PMMA coating, resulting in successful PDMS binding. Nevertheless, the experiments with water solvent suffered unstable operation when the device was in

contact with water for more than several tens of minutes. We are modifying our device so that high-k dielectric insulating layers (e.g., HfO_2, TiO_2, HfO_2, and Al_2O_3) cover the channel, as previously proposed.[49] The protection layer should contribute to the duration of the device. At the same time, we have developed an optical method to execute chemical recognition of the adsorbed molecules on the channel. In the process, we inject a monochromatized UV-Vis light corresponding to the HOMO-LUMO excitation energy to enhance the occupation of the electron in the unoccupied state of the MoS_2 channel through the charge transfer from the molecule to the MoS_2. This technique can be applied to attach the molecule specificity to the device.[50]

Conclusion

In summary, we investigated the biosensor behavior of MoS_2-FET for the UA molecule.

Our FET was designed so that the electrodes of the source and drains are protected by PMMA and only a center of the MoS_2 channel contacts with the solution through the via hole. The equipped microfluidic channel controls the solution's flow, which realizes the evaporation free and constant flow environment. The IPA was used as a solvent. The pure IPA flow shifted the I_d-V_g curve towards higher V_g direction suggesting electron acceptor nature of the IPA. When we switch the syringe of IPA to UA solution, the I_d-V_g plot shifts towards the left, indicating the electron donor type behavior. We execute the VASP DFT calculation which supports this behavior. The I_d-V_g plots shift with UA concentration, whose shift is numerically estimated by measuring the threshold voltage. The ΔV_g changes linearly with UA concentration up to 1 μM of UA concentration, and we estimate the detection limit of 60 nM. The sensor shows a good reproducibility for cycles of 100 nM UA solution flow and IPA washing in a repeated manner. This experiment indicates a potential application of the MoS_2-FET for *in vivo* monitoring of UA molecules.

Author contribution

MN: Conceptualization, experimentalizing, writing; HW, TT: methodology; ZW: visualization; YS: experimentalizing; MM: methodology; AA: visualization; MF, AH: instrumentation, experimentalizing; methodology T.K Conceptualization, supervision, resources. editing. All authors have read and approved the final version of the manuscript.

Conflicts of Interest

There are no conflicts to declare.

Acknowledgment:

This study was supported in part by Grant-in-Aid for Scientific Research (S) (No.19H05621) (for TK). The part of this work was conducted at NIMS Nanofabrication Platform, supported by "Nanotechnology Platform Program" of the Ministry of Education, Culture, Sports, Science and Technology (MEXT), Japan, Grant Number JPMXP1222NM0034. This work was supported by JST SPRING, Grant Number JPMJSP2114.

References

1. Q. Yue, Z. Shao, S. Chang and J. Li, *Nanoscale Res. Lett.*, 2013, **8**, 425.
2. F. Schedin, A. K. Geim, S. V. Morozov, E. W. Hill, P. Blake, M. I. Katsnelson and K. S. Novoselov, *Nat. Mater.*, 2007, **6**, 652-655.
3. K. Huang, M. Zhao, B. Sun, X. Liu, J. Liu, H. Chang, Y. Zeng and H. Liu, *ACS Appl. Electron. Mater.*, 2020, **2**, 971-979.
4. E. S. Kadantsev and P. Hawrylak, *Solid State Commun.*, 2012, **152**, 909–913.
5. D. Sarkar, W. Liu, X. Xie, A. C. Anselmo, S. Mitragotri and K. Banerjee, *ACS Nano*, 2014, **8**, 5367.
6. B. Radisavljevic and A. Kis, *Nat. Mater.*, 2013, **12**, 815–820.
7. B. Radisavljevic, A. Radenovic, J. Brivio, V. Giacometti and A. Kis, *Nat. Nanotechnol.*, 2011, **6**, 147-150.
8. B. Radisavljevic, A. Radenovic, J. Brivio, V. Giacometti and A. Kis, *Nat. Nanotechnol.*, 2020, **13**, 1644-1650.
9. D. Kiriya, M. Tosun, P. Zhao, J. S. Kang and A. Javey, *J. Am. Chem. Soc.*, 2014, **136**, 7853−7856.
10. X. Chen, C. Liu and S. Mao, *Nano-Micro Lett.*, 2020,**12**, 95.
11. X. Chen, S. Hao, B. Zong, C. Liu and S. Mao, *Biosens. Bioelectron.*, 2019, **145**, 111711.
12. M. Ikram, L. Liu, Y. Liu, L. Ma, H. Lv, M. Ullah, L. He, H. Wu, R. Wang and K. Shi, *J. Mater. Chem. A*, 2019, **7**, 14602–14612.
13. P. E. Erden and E. Kiliç, *Talanta*, 2013, **107**, 312-323.
14. B. N. Ames, R. Cathcart, E. Schwiers and P. Hochstein, *Proc. Natl. Acad. Sci. U. S. A.*, 1981, **78**, 6858-6862.
15. K. L. Rock, H. Kataoka and J. J. Lai, *Nat. Rev. Rheumatol.*, 2013, **9**, 13-23.
16. D. Dussossoy, M. L. Py, G. Pastor and X. Boulenc, *J. Pharm. Sci.*, 1996, **85**, 955-959.
17. W. L. Nyhan, *Journal of Inherited Metabolic Disease*, 1997, **20**, 171–178.
18. F. Wu, Y. Huang and Q. Li, *Anal. Chim. Acta*, 2005, **536**, 107-113.
19. I. M. Mostafa, M. I. Halawa, Y. Chen, A. Abdussalam, Y. Guan and G. Xu, *Analyst*, 2020, **145**, 2709-2715.
20. D. L. Rocha and F. R. P. Rocha, *Microchem. J.*, 2010, **94**, 53-59.
21. D. Swinson, J. Snaith, J. Buckberry and M. Brickley, *Int. J. of Osteoarchaeol.*, 2008, **20**, 135-143.
22. Y. Liu, H. Li, B. Guo, L. Wei, B. Chen and Y. Zhang, *Biosens. Bioelectron.*, 2017, **91**, 734-740.

23. F. Mazzara, B. Patella, G. Aiello, A. O'Riordan, C. Torino, A. Vilasi and R. Inguanta, *Electrochim. Acta*, 2021, **388**, 138652.
24. X. J. Huang, H. S. Im, O. Yarimaea, J. H. Kim, D. H. Lee, H. S. Kim and Y. K. Choi, *J. Phys. Chem. B*, 2006, **110**, 21850-21856.
25. V. Pavlíček, P. Tůma, J. Matějčková and E. Samcová, *Electrophoresis*, 2014, **35**, 956-961.
26. H. Li, Z. Yin, Q. He, H. Li, X. Huang, G. Lu, D. W. H. Fam, A. I. Y. Tok, Q. Zhang and H. Zhang, *Small*, 2012, **8**, 1-159.
27. J. Ryou, Y. S. Kim, K. C. Santosh and K. Cho, *Sci. Rep.*, 2016, **6**, 29184.
28. D. Wu, H. F. Lu, H. Xie, J. Wu, C. M. Wang and Q. L. Zhang, *Sensors Actuators, B Chem.*, 2015, **221**, 1433-1440.
29. R. Sha, N. Vishnu and S. Badhulika, *Sensors and Actuators B: Chem.*, 2019, **279**, 53-60.
30. A. M. Goodman, M. D. Wheelock, N. G. Harnett, S. Mrug, D. A. Granger and D. C. Knight, *Neuroscience*, 2016, **339**, 396-401.
31. D. J. Beebe, G. A. Mensing and G. M. Walker, *Annu. Rev. Biomed. Eng.*, 2002, **4**, 261-286.
32. E. K. Sackmann, A. L. Fulton and D. J. Beebe, *Nature*, 2014, **507**, 181-189.
33. Y. Jiang, S. Zou and X. Cao, *Anal. Methods*, 2016, **8**, 6668-6681.
34. B. K. Gale, A. R. Jafek, C. J. Lambert, B. L. Goenner, H. Moghimifam, U. C. Nze and S. K. Kamarapu, *Inventions*, 2018, ***3***, 60.
35. S. M. Scott and Z. Ali, *Micromachines*, 2021, **12**, 319.
36. N. T. Trung, M. I. Hossain, M. I. Alam, A. Ando, O. Kitakami, N. Kikuchi, T. Takaoka, Y. Sainoo, R. Arafune and T. Komeda, *ACS Omega*, 2020, **5**, 28108-28115.
37. S. Das, H. Chen, A. V. Penumatcha, J. Appenzeller, *Nano Lett.,*2013, **13**, 100-105.
38. G. Kresse and J. Furthmüller, *Comput. Mater. Sci.*, 1996, **6**, 15-50.
39. D. Joubert, *Phys. Rev. B - Condens. Matter Mater. Phys.*, 1995, **59**, 1758-1775.
40. J. P. Perdew, K. Burke and M. Ernzerhof, *Phys. Rev. Lett.*,1996, **77**, 3865-3868.
41. K. Momma and F. Izumi, *J. Appl. Crystallogr.*, 2011, **44**, 1277-1276.

42. B. Pullman and A. Pullman, *Proc. Natl. Acad. Sci.*, 1958, **44**, 1197-1202.
43. I. Langmuir, *J. Am. Chem. Soc.*, 1918, **40**, 1361-1403.
44. S. Azizian, S. Eris and L. D. Wilson, *Chem. Phys.*, 2018, **513**, 99-104.
45. M. S. Al Mamun, Y. Tanaka, H. Waizumi, T. Takaoka, Z. Wang, M. I. Alam, A. Ando, M. Fukuyama, A. Hibara and T. Komeda, *Phys. Chem. Chem. Phys.*, 2020, **22**, 27724-27731.
46. H. Bourbaba, C. Ben Achaiba and B. Mohamed, in *Energy Procedia*, 2013, **36**, 331-237.
47. B. Ryu, H. Nam, B.-R. Oh, Y. Song, P. Chen, Y. Park, W. Wan, K. Kurabayashi and X. Liang, *ACS Sensors*, 2017, **2**, 274–281.
48. J. H. Park, D. K. Hwang, J. Lee, S. Im and E. Kim, *Thin Solid Films*, 2007, **515**, 4041-4044.
49. Y. Y. Illarionov, T. Knobloch, M. Jech, M. Lanza, D. Akinwande, M. I. Vexler, T. Mueller, M. C. Lemme, G. Fiori, F. Schwierz and T. Grasser, *Nat. Commun.*, 2020, **11**, 3385.
50. M. I. Alam, T. Takaoka, H. Waizumi, Y. Tanaka, M. S. Al Mamun, A. Ando and T. Komeda, *RSC Advances*, 2021, 11, 26509-26515.